CCD QE in the Soft X-ray Range

Ian Moody[a], Marc Watkins[a], Ray Bell[a]
Matthew Soman[b], Jonathan Keelan[b], Andrew Holland[b]
[a]e2v, 106 Waterhouse Lane, Chelmsford, Essex, CM1 2QU, UK
[b]CEI, The Open University, Milton Keynes, MK7 6AA, UK

ABSTRACT
e2v has previously provided back-illuminated CCDs for several solar observation projects, resulting in a number of key articles on CCD QE in the soft X-ray region. To update these, e2v has arranged for tests on X-ray optimised EMCCDs at a synchrotron. These have shown QE of at least 45% from 40 eV to 2000 eV, with Enhanced process devices having significantly higher QE than Basic process. The measured values were similar to data published from the SDO SXI mission, showing that the e2v process has been stable over many years.

The soft X-ray QE measurements show a reasonable fit to the simple layer model for energies > 600 eV. For energies < 100 eV, measurements show slightly lower QE than the model prediction for both Basic and Enhanced processes. For energies 100 eV to 600 eV, measurements show a reasonable fit to the model for the Basic process, but less improvement from the Enhanced process than the model predicts. Comparing the ~80% typical QE for UV-optimised CCDs at 385 nm with the 45% QE measured at 120 eV in this study, there is a discrepancy in QE for two photon energies with the same absorption length measured on CCDs from the same back-thinning process (one type with AR coating, one type without).

Keywords: CCD, CMOS, QE, X-ray, RIXS, EUV, VUV

1. Introduction

Quantum Efficiency (QE) is the ratio of the number of photons detected to the number of photons arriving at the detector surface. Sometimes in the UV, it is taken as the ratio of the number of electrons to the number of photons. For high QE, the detector needs to efficiently absorb the photon and have very few loss mechanisms, so that the signal electron(s) are efficiently collected.

e2v routinely tests the QE in the visible range, but since back-thinned CCDs have a high response over a very wide spectrum, it is e2v's general objective to be able to provide QE values spread out from visible through to X-ray. In this first step, e2v has arranged soft X-ray QE tests at the BESSY II synchrotron, Germany. In the next phase, e2v plans QE tests at e2v in the VUV range from 120 nm to 250 nm, on the WUVS mission CCD [1].

The soft X-ray QE work described below has been carried out in collaboration with the Centre for Electronic Imaging (CEI) at the Open University (www.open.ac.uk/cei), which is supported by e2v (www.e2v.com). The camera for the QE measurements was purchased by the CEI from XCAM Ltd (www.xcam.co.uk). All the CCDs were taken from standard production streams at e2v.

1.1 Background of Soft X-ray (SXR) Imaging at e2v

e2v has so far developed three different CCD technologies for the detection of soft X-rays:-

a. Back-thinned CCDs with no Anti-Reflective (AR) coating. These have been used in several solar observation space missions including SDO, SXI (solar X-ray imager), Stereo SECCHI and HINODE [2] [3] [4] [5][6]. These CCDs have also been used in synchrotron applications, such as Resonant Inelastic X-ray Scattering (RIXS) [7]
b. Open electrode CCDs with an aperture in the polysilicon electrodes to allow soft X-ray photons to be absorbed in the silicon: used in the XMM space mission [8]

c. Swept Charge Devices: large area single pixel detectors for photodiode arrays: used in the Chandrayaan and HXMT space missions [9]

The associated space missions have resulted in a number of key articles in the literature on soft X-ray imaging [2][3][4][5][6] [8] and the technology of back-thinned CCDs [10]. e2v has also processed back-illuminated CMOS sensors for soft X-ray imaging [11] and for a space mission, with calibration using the characteristic soft X-ray spectrum from an Iron-55 source [12].

1.2 Aims of the Soft X-ray QE Study

- To generate a simple layer model for QE in the soft X-ray range.
- To compare the fit of this model to QE measured in the soft X-ray range.
- To update the soft X-ray QE data on e2v CCDs in the literature.
- To compare the new measurements against those taken in the 1990s for the SDO mission.
- To make comparisons about QE and absorption processes for the visible and soft X-ray ranges.

1.3 Comparison between Visible and Soft X-ray Characteristics

e2v offers both Basic and Enhanced back-thinning processes. Both of these have a shallow p+ layer at the surface, but for the Enhanced process, the p+ layer is thinner, to bring the potential peak as close to the surface as possible. This minimises any 'dead' layer, which is critical to achieving high QE for blue, UV and soft X-rays. In order to help with the modelling and predictions of QE for the soft X-ray range, it is instructive to compare the interaction of visible and soft X-ray photons with the detector:-

- In the visible range, it is advantageous to match the refractive indices of silicon and air with an anti-reflective (AR) coating, but in the soft X-ray range, these coatings have no effect, other than absorption.
- The QE for soft X-ray photons may be reduced by, for example, a native oxide film on the silicon surface, as well as a surface recombination layer in the silicon.
- In the visible range, one photon produces one signal electron. In the soft X-ray range, one photon produces a cloud of many electrons: over 500 for the highest energy in the range studied.
- Both blue and soft X-ray photons have short absorption depths. The shortest absorption depth in the soft X-ray range studied was at ~120 eV. A 380 nm visible photon has approximately the same absorption depth as a 120 eV X-ray photon.
- A photon in the 100 nm to 300 nm UV range has an absorption depth which is even shorter, by an order of magnitude, compared to a 380 nm visible or a 120 eV X-ray photon. On this basis, it would be reasonable to expect surface recombination layers on the surface of the detector to reduce the QE more significantly for 100 nm to 300 nm UV photons, than for 120 eV soft X-ray photons.

Absorption Depth for Soft X-ray and Visible Photons in Silicon [13][14]

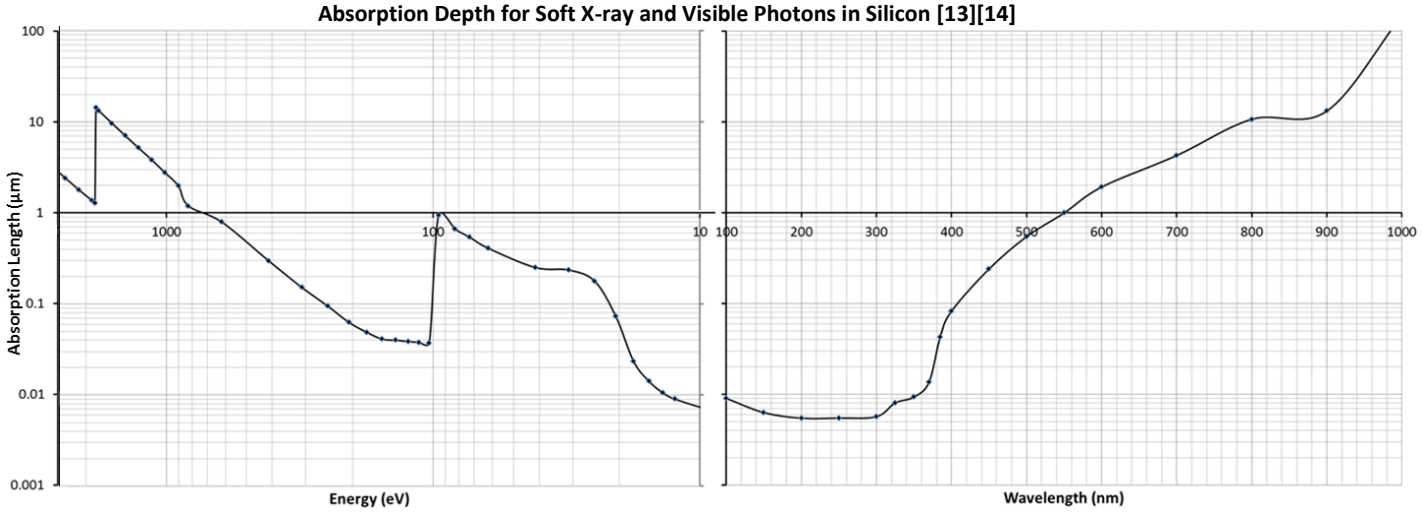

2. Optimisation, Measurement and Modelling of Visible Band QE at e2v

2.1 Introduction

In the visible range, achieving high QE starts with an anti-reflection coating matching the refractive index of the silicon to that of air, to reduce reflection. The average depth of the absorption is also relevant to the detector performance. In general, mid-band (~550 nm) wavelengths have an absorption depth of about 1 µm, and near-IR (~800 nm) wavelengths about 10 µm. This compares to a typical CCD active thickness of 16 µm (standard epi) or 40 µm (deep depletion).

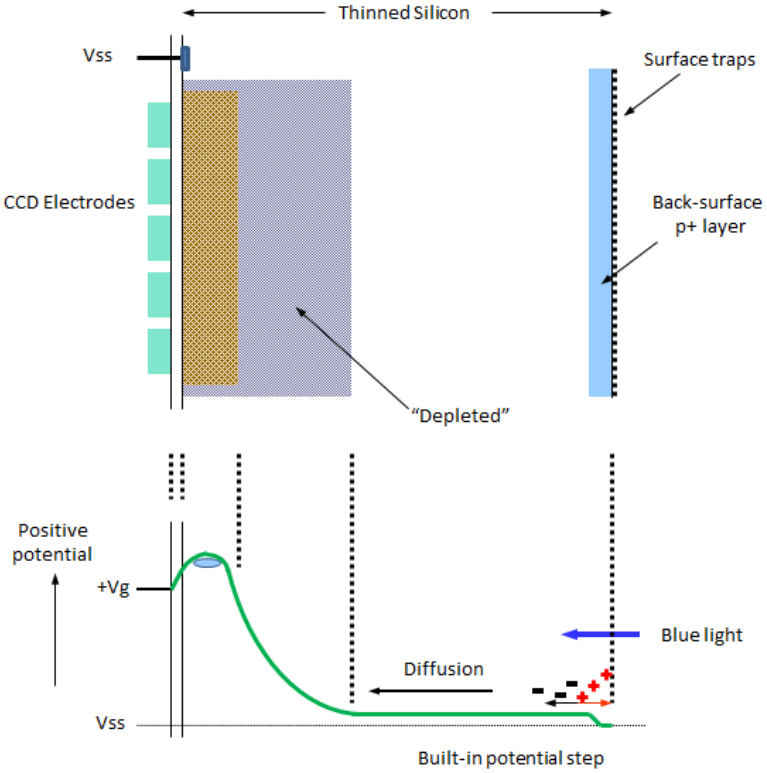

Below 350 nm, the absorption depth becomes very short: less than 0.01 µm. Rather than ensuring strong absorption and high QE, this aspect actually provides a significant challenge due to surface effects. In back-illuminated CCDs, the back surface must be passivated to achieve high QE. This prevents recombination of photo-generated signals at the etched surface, which has a high density of traps. The passivation method used by e2v is to form a p+ layer by ion-implantation, and activate this by a UV laser pulse, which melts only a shallow surface layer. Provided the p+ layer is made thin enough, good QE below 350 nm is obtained.

2.2 The e2v model for Visible Band QE

e2v maintains an in-house model which calculates the QE of a back-illuminated CCD between 200 nm and 1100 nm. With one or two exceptions, e2v tests the QE of every back-illuminated CCD it manufactures, and these measurements are compared to the model on a regular basis. The model takes account of:-

- Silicon and AR coating layer refractive indices
- Silicon absorption coefficient, including temperature dependence
- Back-thinning process (Enhanced, Basic) dependence for wavelengths below 500 nm
- Reflection from the front and back surfaces of the silicon

It is e2v's convention to assume one signal electron is generated per photon down to 200 nm.

Modelled QE for Mid-Band AR-coated, Basic Process, 16µm epi, Back-Illuminated CCD at -20°C

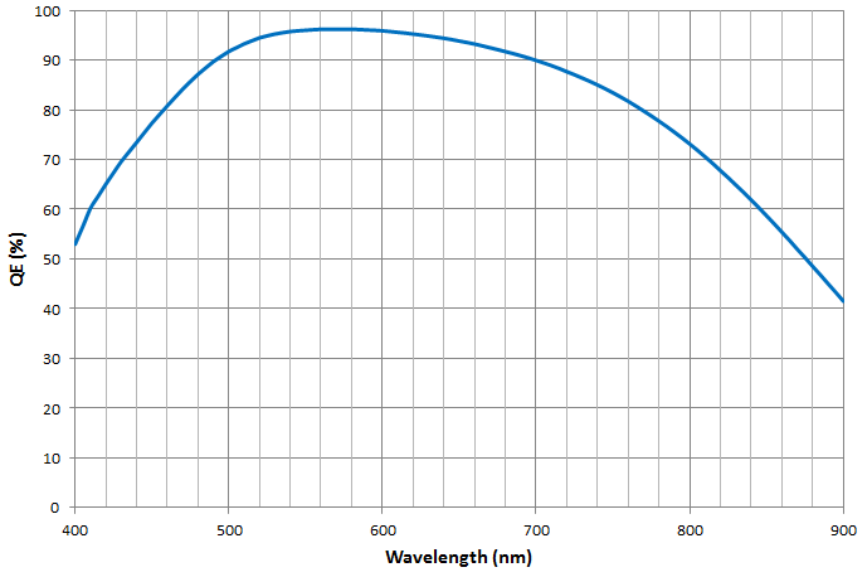

3 X-ray QE

3.1 Medium Energy X-ray QE

For X-rays, anti-reflection coatings have no effect other than absorption, and refractive indices are of no use in the calculation of QE. Instead, at least for the medium energy X-ray region from 2 keV to 20 keV, absorption depth is the primary parameter. It is straightforward to base the QE calculation on the silicon absorption [14][15][16][17][18], and the actual QE of e2v CCDs is close to this curve:-

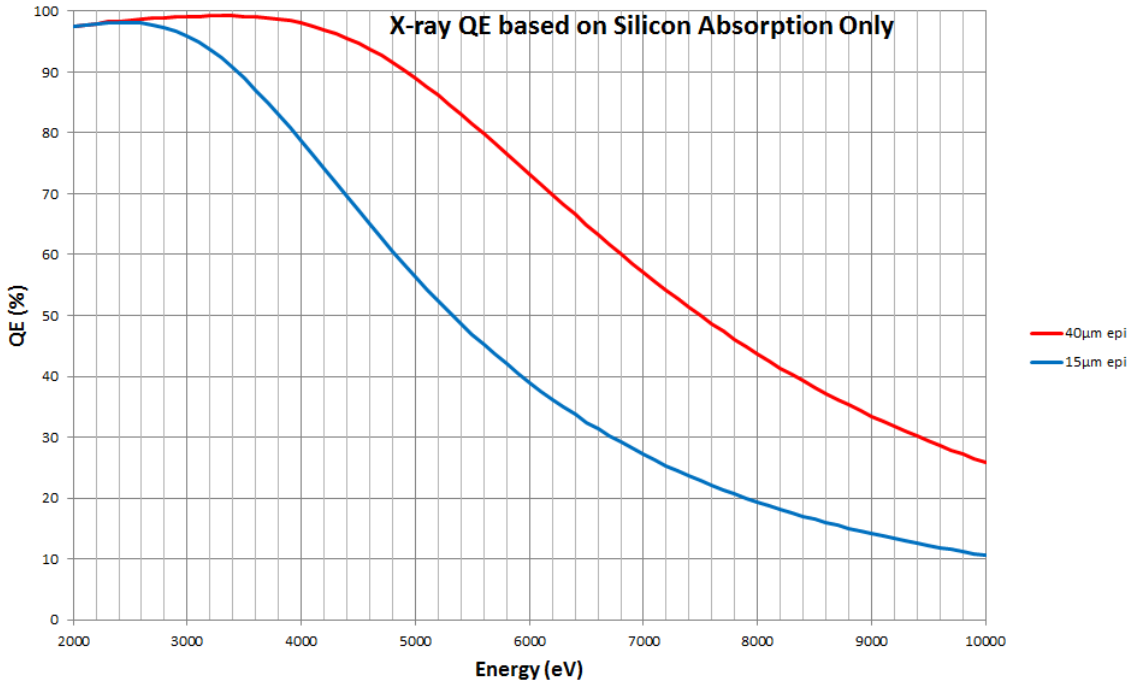

3.2 Soft Energy X-ray QE

In the soft X-ray region, from 20 eV to 2000 eV, basing the QE only on the silicon absorption leads to significant errors since the typical absorption length is so short (less than 1 µm) and photons may be absorbed in any dielectric layers on the silicon surface. If transmitted through all surface layers, photons are likely to be absorbed very close to the detector surface, where surface effects have a high impact on the QE.

3.3 The Simple Layer X-ray QE Model

The simple X-ray QE model simulates layers of varying thickness and materials. X-ray attenuation lengths are taken from data tables [14][15][16][17][18] and used to calculate the X-ray absorption in each of the layers. The final layer (here shown in yellow) is then considered to be the sensitive region. The ratio of the initial intensity of the X-ray beam to the intensity absorbed in the sensitive layer gives the QE.

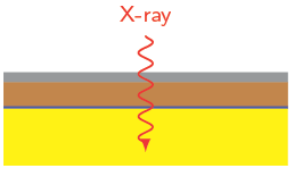

The attenuation of a single energy X-ray beam through material of thickness *t* can be expressed as:

$$I = I_0 e^{-t/\lambda(E)}$$

Where λ(*E*) is the X-ray attenuation length of the material for X-rays of energy *E* and I_0 is the incident intensity.

The remaining intensity of an X-ray beam which has travelled through a series of material layers *i* can be written as:

$$I_T = I_0 e^{-\sum_i t_i/\lambda_i(E)}$$

Where I_T is the intensity which reaches the sensitive detector region after passing through a series of material layers.

To calculate the quantum efficiency of the detector, the proportion of the beam which is absorbed in the sensitive region must be found. The modelled detector QE at X-ray energy *E* can then be expressed as:

$$QE(E) = \frac{I_T}{I_0}\left(1 - e^{-t_s/\lambda_s(E)}\right)$$

Where subscript s denotes the properties of the final, sensitive layer in the detector and I_0 is the intensity of the original X-ray beam.

3.4 The X-ray Absorption Process for Silicon

The general reduction in X-ray absorption with increasing energy is interrupted by a sharp rise when the energy is equal to the binding energy of an electron shell. This energy is the least at which a vacancy can be created in the particular shell and is referred to as the 'edge' energy.

The silicon atom has a 3 electron shells, known as K, L and M. Electrons in the K shell have the lowest potential and so require the highest energy to be ejected (1839 eV). Vacancies created in a lower shell will promptly be filled with an electron from a higher shell. For the K shell, an electron can be ejected to create a vacancy, which will then be accompanied by either the emission of an X-ray photon (X-ray fluorescence, with characteristic photon energy) or the transfer of energy to another (Auger) electron, which is then emitted.

The main region of interest of this paper is below the K edge at 1839 eV. The absorption in silicon in this region is dominated by the emission of energetic electrons, since the probability of X-ray fluorescence is much less than 1% [19]. For an incident X-ray photon with energy between the L_I and K edges the absorption is distributed between the L_I shell at 148.7 eV, the L_{II_III} shell at 99.2 eV and the M_I shell at 11.4 eV.

Bohr Model of the Silicon Atom

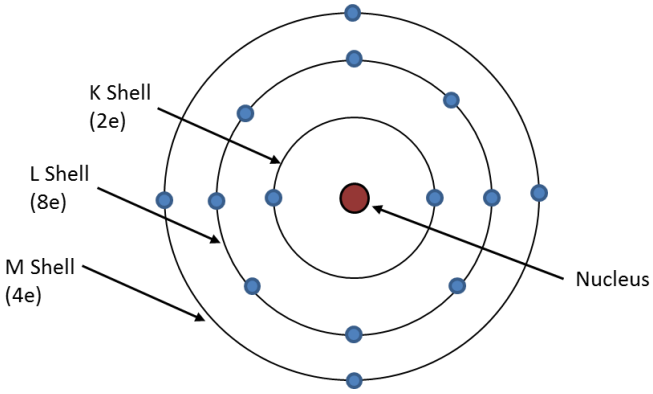

On average, 3.6 eV is required for each free signal electron emitted from the silicon atom after absorption of an X-ray photon [20], with variance as per the Fano factor. The complete absorption of a 500 eV X-ray photon produces on average approximately (500 / 3.6) = 139 signal electrons, but a large number of steps are involved in this absorption. The absorption process is followed until all vacancies are transferred to the lowest energy outermost M shell.

In the first absorption effect, a photoelectron is emitted with energy equal to the X-ray photon energy minus the energy required to eject an electron from the shell. The ejected high energy electron then interacts with neighbouring atoms to produce a cascade of electrons. Each successive photoelectron has lower energy by an amount equal to the shell vacancy energy.

For each of the interactions emitting a photoelectron, the atom in an excited state undergoes a transition to a lower state by the emission of an Auger electron. At the same time as a photoelectron is emitted, an Auger electron is also emitted. In ~10% of these emissions, there is also emission of lower energy electrons due to an effect called shake-off [19]. This occurs when there is an abrupt change in atomic potential at photo-ionisation and Auger electron emission.

Expected Electron Cascade after Absorption of a 500 eV X-ray Photon [19]

		Electron Emission for 500 eV X-ray Photon		
Shell	**Shell vacancy (eV)**	**Auger Electron (eV)**	**Photoelectron (eV)**	**~9.5% Probability Shake-off Electron (eV)**
L_I	148.7	132	351.3	6.25
L_I	148.7	132	202.6	6.25
			53.9	
L_{II_III}	99.2	83	400.8	6.55
L_{II_III}	99.2	83	301.6	6.55
L_{II_III}	99.2	83	202.4	6.55
L_{II_III}	99.2	83	103.2	6.55
			4.0	

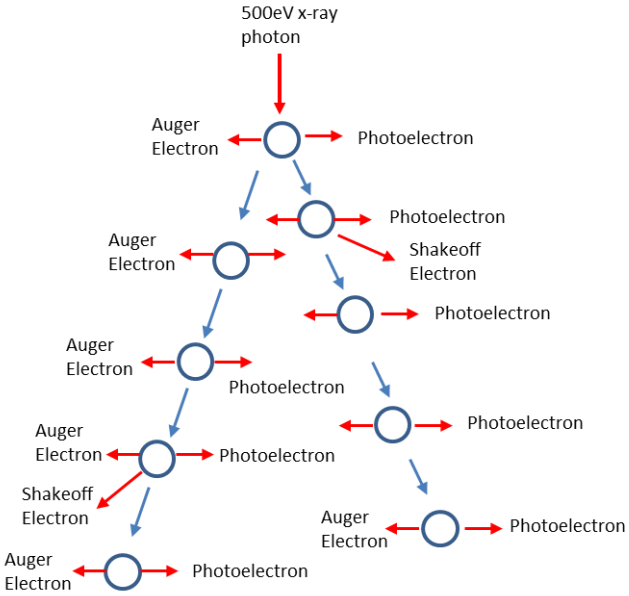

Overall, it can be seen that there are many stages involving energetic, so-called 'hot', free electrons. These electrons are emitted uniformly in all directions, centred on the interaction site of the incident X-ray photon, forming a cloud of signal electrons. This expands in size due to mutual electrostatic repulsion and diffusion, before it is collected as a signal.

3.5 Charge Collection Efficiency for X-ray Photons

The pattern of white dots on a dark image generated by X-ray photons emitted from an Fe55 source is a familiar one for many people. The signal level can be used as a calibration for the system gain in electrons per count. The Fe55 source produces mainly 5.9 keV X-ray photons. When these are absorbed in the CCD, they give rise to a charge cloud which, when collected, is often larger than the typical pixel size of 13 µm, even when the CCD is well depleted, in NIMO mode. Split-charge events, with signal shared between two or more pixels, are also often seen on the dark image.

The size of the initial charge cloud, in the instant when first generated by the X-ray photon, is not such a familiar topic. The range of the primary photoelectron is a function of its energy [21][22][23]. At the extent of this range, the energetic electron has normal energy level. The range describes the radius of the initial charge cloud. For X-ray energies in the 100 eV to 300 eV range, the initial charge cloud radius, when the photon is converted into electrons of normal energy level, is very small: 4 nm or less [21][22][23]. By comparison, the absorption depth at ~100 eV is approximately 40 nm. The size of the initial charge cloud increases after generation, due to diffusion and mutual repulsion under the influence of the electric field from the collection electrodes.

The charge is swept away from the detector surface by the potential gradient from the p+ layer. There may be a random walk of signal electrons in the un-depleted depth but, as with visible photons, this should result in signal in the adjacent, rather than the actual pixel, and not in recombination losses.

Back-Illuminated CCD in Cross Section

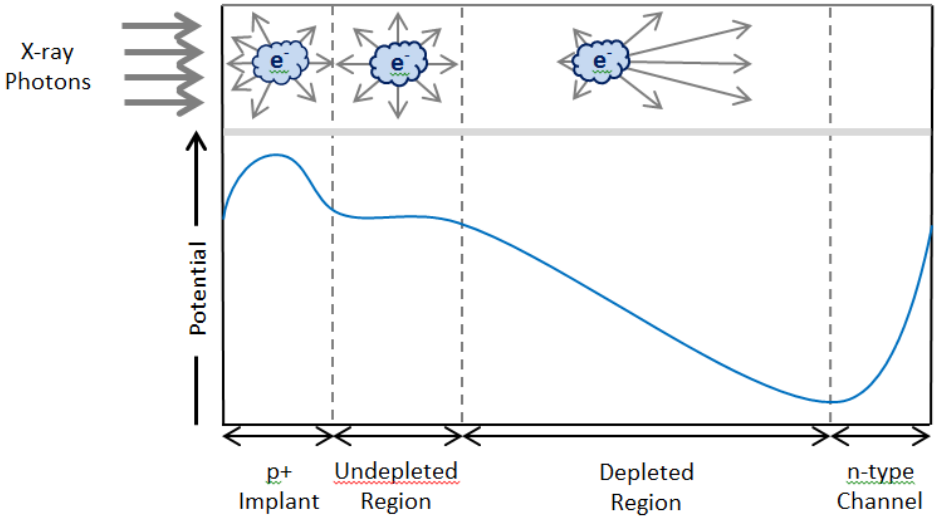

The extra analysis required regarding interaction of the initial charge cloud with the surface or the p+ layer, or of the incident photon with a partial charge generating / recombination layer adjacent to the p+ layer is outside the scope of this paper, but is a planned next step. The main effect which could account for QE and signal loss can be simply expressed as absorption within a surface dead layer or within the p+ layer, but the accuracy of this approach may not be high.

4. Soft X-ray QE Tests at BESSY

4.1 Device

The device type chosen for QE testing was the e2v CCD97 electron multiplication device [24]. The sub-electron readout noise enabled photon counting down to the limit of the BESSY beamline of ~40 eV, allowing for possible 2×2 pixel split charge events with only ~3 electron charge per pixel.

CCD97s were fabricated in both Basic and Enhanced Process forms. Final processing was slightly non-standard and aimed at soft X-ray imaging, with no-AR coating, and no store-shield. Careful handling ensured that surface contaminants were minimised. The build standards were carefully monitored and recorded.

4.2 Camera

The camera used to operate the CCD97 was based on a vacuum flange arrangement, with the minimum of components on the vacuum side of the flange, and with the flange compatible with the port on the BESSY beamline. Extensive pre-BESSY testing ensured stability of EM gain (typical value ×200) and CCD temperature (typical value -45 °C). Careful handling was used throughout, to minimise contaminants, and ensure compatibility with the high cleanliness vacuum environment at BESSY.

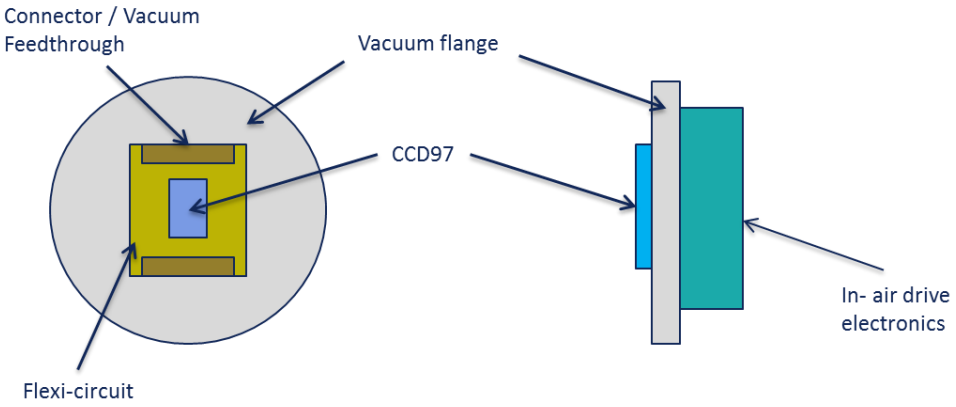

4.3 Experimental Arrangement at BESSY

Detailed planning for the tests at BESSY included the assessment of risks, and the generation of a test procedure and test plan. This included a detailed timetable of events with contingency planning, to ensure the best use of beam time. To further minimise the possibility of contaminants on the surface of the CCD97, a liquid nitrogen trap was located adjacent to the device, with gate valve isolation for device changing.

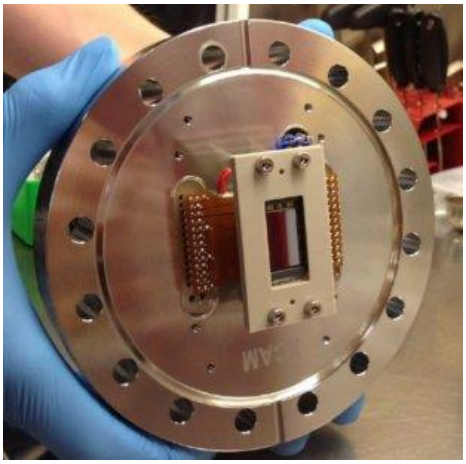

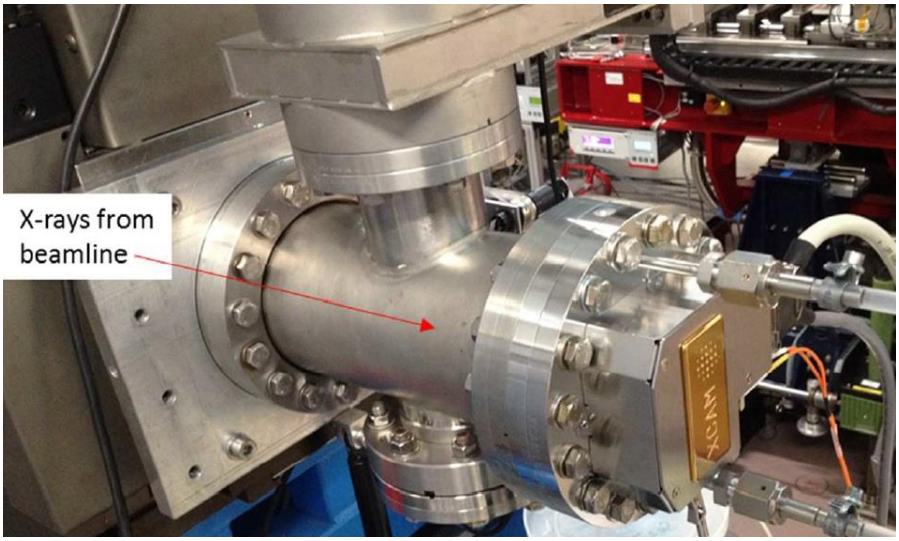

4.4 Test Procedure at BESSY

The BESSY II synchrotron operates in top-up mode. The circulating current slowly decays over time, and new charge is injected every ~100 seconds, so that the average current is constant over long periods. Since this top-up could have affected the QE measurements, the fractional change in the ring current was calculated. The conclusion was that the vast majority of time was spent in the slow decay mode, with varying levels of top-up. Over the typical measurement period of 200 seconds, the net change in beam current was observed to be negligible.

At each setting of X-ray energy, a measurement was taken with a reference diode, before and after the CCD was exposed, to obtain the power incident on the detector, and track any changes in the beam power during the QE test duration. The diode was moved into the beam path whilst the beam shutter was closed. The shutter was then opened, and a measurement taken, before finally closing the shutter and taking another dark reference measurement. The average dark reference value was then subtracted from the average measurement value, giving an average diode reference current. The beamline radiant power was adjusted at each setting of X-ray energy, to provide a measurable signal above the diode's dark current. The aim was to set up a low beam power and a photon-counting regime for the CCD97.

The CCD97 Rϕ2HV voltage was adjusted at the beginning of the day to provide a gain of approximately ×200, as measured by a gain versus HV curve using optical light.

The images generated during the X-ray tests were mostly in a TDI (Time Delay and Integrate) mode, with continuous forward clocking of the CCD image area, and continuous readout of the CCD register. The TDI mode had an image width of 552 columns, in order to minimise the effective readout time per row and maximise the opportunities for photon counting. A total of 8,000 rows were read out per image, including signal generated in both the store and image regions during a short initial integration time.

For measurement of QE, the signal per column was produced by digitally summing all the signal in that column from the TDI region (parallel overscan). Background dark signal and electrical offset was subtracted on a column-by-column basis, using dark reference frames collected throughout the experiment. The summing of signal charge across rows and columns enabled signal charge collection per unit time to be measured - a value unaffected by X-ray events split over multiple pixels. Since the area illuminated by the X-ray beam was relatively small, it was assumed that the entire X-ray beam was collected by the CCD, and also by the photodiode, and so no scaling for area was necessary.

The location and alignment of the X-ray beam with respect to the CCD imaging area was observed in the image and store regions recorded before the TDI region. The ~1 s integration time led to significant pileup, but the beam location and alignment was still clear. The TDI region had lower flux, and so was more suitable for studying individual X-ray events.

The analysis procedure for determining the X-ray power detected in the CCD was as follows:

1. Measure the dark background level for each column in the TDI region using dark frames.
2. Subtract the background level from the TDI region, column by column.
3. Add up the signal observed in the background-subtracted TDI region and divide by the number of rows, to give the signal per row (in Digital Numbers, DN), then divide by the line read time (375 µs) to determine the signal measured by the CCD97 per second.
4. Use the low-flux regions to extract isolated X-ray events to determine the calibration (e-/DN).
5. Using the results from steps (3) and (4), as well as the incident X-ray energy, determine the number of observed photons per second.
6. Compare the number of photons observed per second in the CCD to the reference power from the reference diode to determine the QE.

5. Soft X-ray Quantum Efficiency (SXRQE) Results

The CCD97 devices which were tested at BESSY are shown in the table below:-

Device Serial No.	Process	Marker in Curve
15051-12-39	Basic	Blue
15051-12-44	Basic	Blue
15051-7-3	Enhanced	Orange
15051-7-7	Enhanced	Orange

The QE values measured at BESSY are presented in the curves below:-

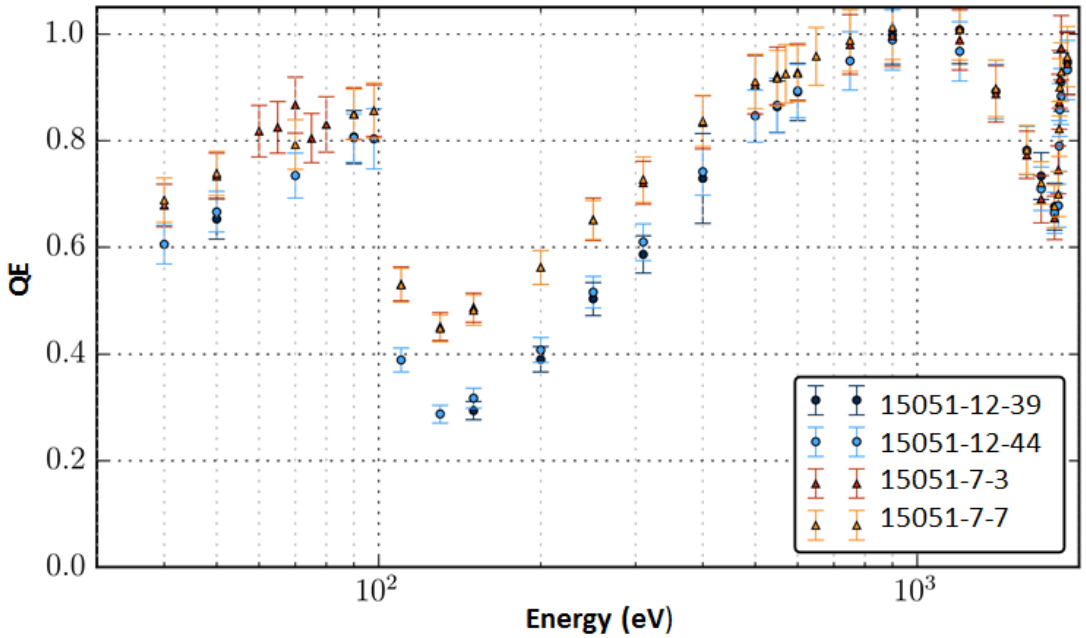

5.1. Analysis of Data & Discussion of SXRQE Results

The soft X-ray QE was successfully measured for 4 off e2v CCD97s at BESSY in a single test campaign over several days. The 40 eV to 2 keV range was explored at multiple energies, with no 'dead-spots' in CCD response seen in this range. The X-ray absorption edges at ~100 eV and ~1800 eV were well resolved. There were no signs of drift in the measurements due to either the CCD or the camera, showing very good cleanliness standards and low levels of molecular contamination.

5.2 Comparison to QE Measured to Data from the SDO / SXI Mission

The measured values for the Enhanced process devices were similar to data from the SDO SXI mission [2][3][10]. This shows that the e2v process has been stable over many years.

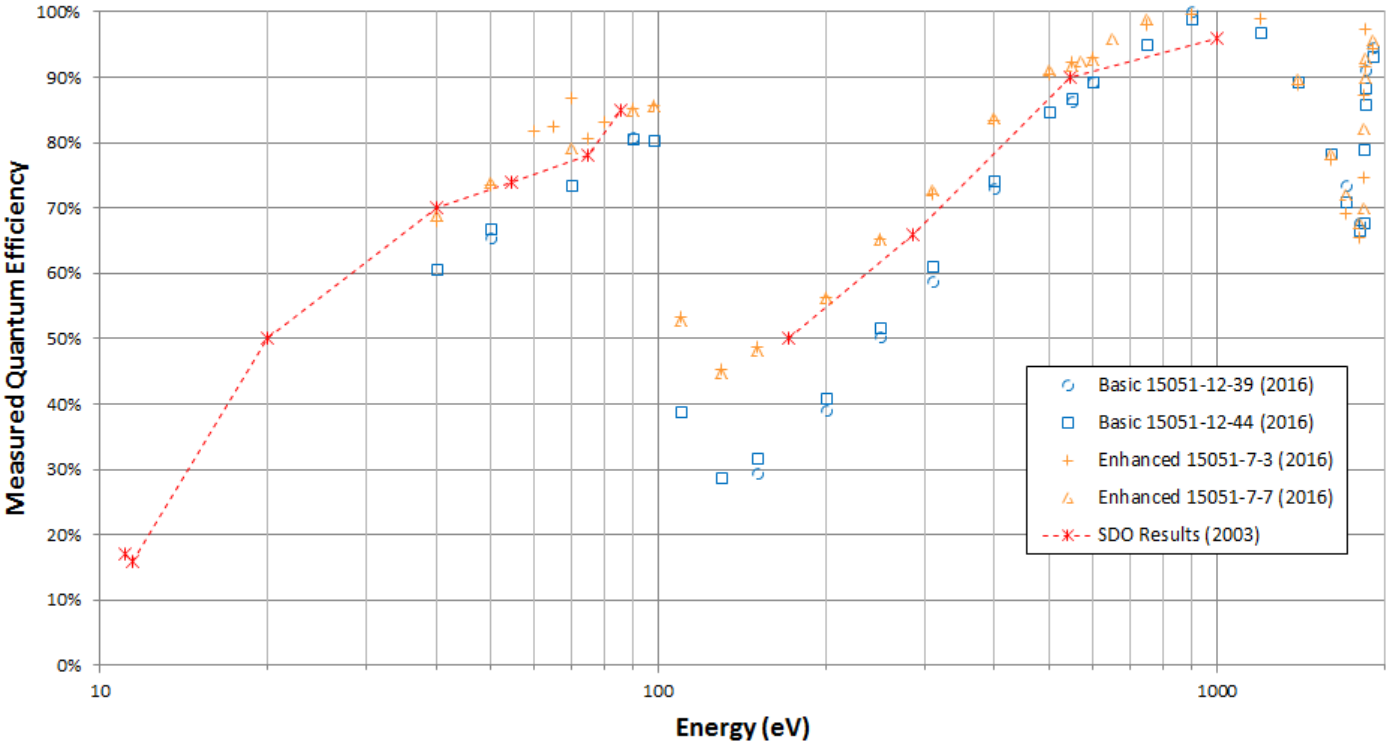

5.3 Comparison of Measured QE Values to the QE Model

Measured and Predicted Values for Basic Process

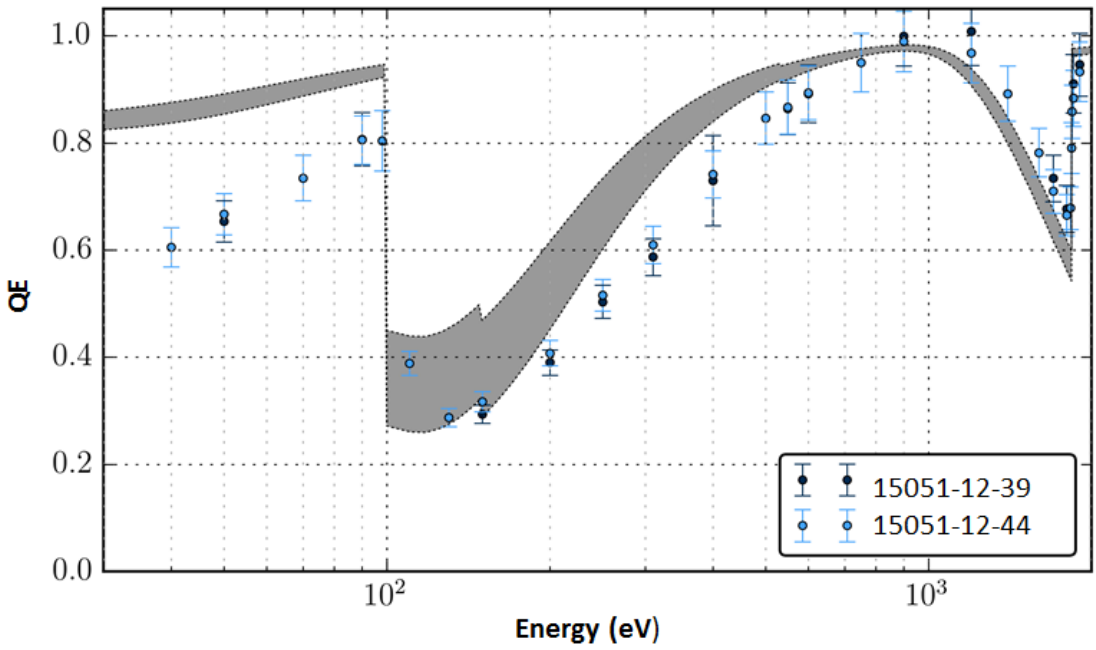

Measured and Predicted Values for Enhanced Process

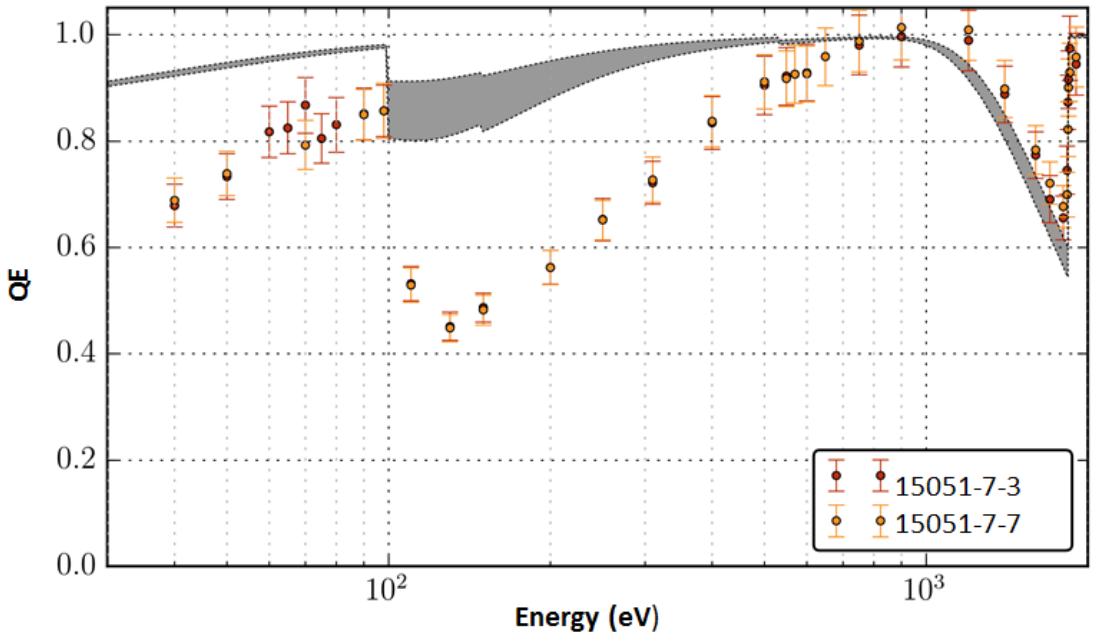

Energies < 100 eV

Measurements show slightly lower QE than the model prediction for both Basic and Enhanced processes. The similarity of performance for both processes may indicate that the loss of QE is due to a similar absorbing film on the silicon surface for both device types. This could be a thicker silicon oxide layer than the assumed native oxide or possibly a contamination film (despite the precautions taken). Future measures to improve this could include ion beam etching plus analysis to confirm the thickness of the silica layer after final processing.

Energies 100 eV to 600 eV

The measurements show a reasonable fit to the model for the Basic process, but far less improvement from the Enhanced process than the model predicts. As the oxide and possible contaminant films on the surface would affect both process variants, it is believed that the recombination of signal at the silicon surface has not been reduced as much as predicted by the reduction of p+ thickness in the Enhanced process devices.

The soft X-ray QE for Enhanced process reaches a minimum of 45% at 120 eV. The absorption length at this energy is ~40 nm [14][15][16][17][18]. By comparison, measurements on e2v CCDs optimised for UV wavelengths have shown QE values nearly double this. The absorption length at 385 nm is ~40 nm, and at 355 nm is ~10 nm. A UV-optimised CCD for the spectrograph in a European environmental monitoring satellite achieved a typical QE of 83% QE at 385 nm. A UV-optimised EMCCD for LIDAR achieved a typical QE of 80% at 355 nm laser wavelength [25]. Assuming a well-matched AR coating giving low reflectance at 385 nm, 80% QE is in line with the predictions of the simple layer model for ~40 nm absorption length photons. Therefore, there is a discrepancy and inconsistency regarding the QE for two photon energies with the same absorption length and measured on CCDs from the same back-thinning process (one type with AR coating, one type without).

Higher surface recombination is the most likely reason for the difference. We believe that the initial charge cloud formed by an X-ray photon causes the local signal charge density to be temporarily higher than the dopant concentration. This means the electron charge cloud self-shields itself from the electrostatic potential formed by the back surface passivation, so that it is not as effective at repelling the charge away from the back surface. With UV photons, only individual electrons are generated per photon, so there is no self-shielding and the electrostatic potential formed by the gradient of doping concentration is more effective. Such a theory could in future be explored by numerical modelling. Ion beam etching plus analysis of doping concentration

could also be used to confirm the thickness of the p+ layer. It must also be borne in mind there are differences in the build standard of the UV-optimised and the X-ray-optimised detectors. The presence of the AR coating for the UV device may modify the surface recombination properties.

Due to the limited CCD cooling available, Inverted Mode Operation (IMO) was needed for low dark current, and this resulted in low depletion depth. This was not thought to be responsible for reduced charge collection efficiency at the incident face. The summing of signal charge across rows and columns was designed to be unaffected by split charge events. Note that, for different systems, it may be important to preserve spatial information during the signal charge collection, and the combination of increased split events and a threshold for X-ray detection could result in a reduction in the effective system QE.

Energies > 600 eV
The measurements show a reasonable fit to the model for both Basic and Enhanced process.

6. Conclusions

e2v back-illuminated CCD97 EMCCDs have demonstrated QE of at least 45% from 40 eV to 2000 eV, with Enhanced process devices showing significantly higher QE than Basic process. The large number of X-ray energies used in the test allowed the X-ray absorption edges at ~100 eV and ~1800 eV to be well resolved. The measured QE values were similar to data from the SDO SXI mission [2][3], showing that the e2v process has been stable over many years.

The soft X-ray QE measurements show a reasonable fit to the simple layer model for energies > 600 eV. For energies < 100 eV, measurements show slightly lower QE than the model prediction for both Basic and Enhanced processes. This could be a thicker oxide layer than the assumed native oxide or possibly a contamination film.

For energies 100 eV to 600 eV, measurements show a reasonable fit to the model for the Basic process, but less improvement from the Enhanced process than the model predicts. Comparing the ~80% typical QE for UV-optimised CCDs at 385 nm with the 45% QE measured at 120 eV in this study, there is a discrepancy in QE for two photon energies with the same absorption length measured on CCDs from the same back-thinning process (one type with AR coating, one type without). Higher surface recombination is the most likely reason for the difference. We believe that the initial charge cloud formed by an X-ray photon causes the local signal charge density to be temporarily higher than the dopant concentration. This means the electron charge cloud self-shields itself from the electrostatic potential formed by the back surface passivation, so that it is not as effective at repelling the charge away from the back surface. Differences in the build standard of the UV-optimised (AR-coated) and the X-ray-optimised (non-AR-coated) detectors may also modify the surface recombination properties.

7. References

[1] Optical design of WUVS instrument: WSO-UV spectrographs
Mikhail Sachkov; Vladimir Panchuk; Maxim Yushkin; Timur Fatkhullin
Proc. SPIE 9905, Space Telescopes and Instrumentation 2016: Ultraviolet to Gamma Ray, 990537 (18 July 2016); doi: 10.1117/12.2233147

[2] Initial Calibration of the Atmospheric Imaging Assembly (AIA) on the Solar Dynamics Observatory (SDO)
Paul Boerner, Christopher Edwards et al
Solar Phys (2012) 275:41–66 doi: 10.1007/s11207-011-9804-8, 24 May 2011

[3] The Atmospheric Imaging Assembly (AIA) on the Solar Dynamics Observatory (SDO)
James R. Lemen, Alan M. Title et al
Solar Phys doi :10.1007/s11207-011-9776-8, 11 April 2011

[4] THE NOAA GOES-12 Solar X-ray Imager (SXI): 1. Instrument, Operations, and Data
S. M. Hill, V. J. Pizzo, C. C. Balch, D. A. Biesecker, P. Bornmann,
Solar Physics (2005) 226: 255–281
doi: 10.1007/s11207-005-7416-x C, 29 November 2004

[5] The NOAA GOES-12 Solar X-ray Imager (SXI): 2. Performance
V. J. Pizzo, S. M. Hill, C. C. Balch, D. A. Biesecker, P. Bornmann
Solar Physics (2005) 226: 283–315. doi: 10.1007/s11207-005-7417-9 C, 29 November 2004

[6] EUVI: the STEREO-SECCHI Extreme Ultraviolet Imager
Jean-Pierre Wülser, James R. Lemen, Ted D. Tarbella et al
Telescopes and Instrumentation for Solar Astrophysics, edited by Silvano Fineschi, Mark A. Gummin,
Proceedings of SPIE Vol. 5171 (SPIE, Bellingham, WA, 2004) · 0277-786X/04/$15 · doi: 10.1117/12.506877

[7] Developing a CCD camera with high spatial resolution for RIXS in the soft X-ray range.
Soman, M. R.; Hall, D. J.; Tutt, J. H.; Murray, N. J.; Holland, A. D.; Schmitt, T.; Raabe, J. and Schmitt, B.
Nuclear Instruments and Methods in Physics Research Section A: Accelerators, Spectrometers, Detectors and Associated Equipment, 731 pp. 47–52 (2013).

[8] MOS CCDs for the EPIC on XMM
Andrew D. Holland ; Martin J. L. Turner ; Anthony F. Abbey ; Peter J. Pool
Proc. SPIE 2808, EUV, X-Ray, and Gamma-Ray Instrumentation for Astronomy VII, 414 (October 31, 1996);
doi: 10.1117/12.256017

[9] Quantum efficiency measurements in the swept charge device CCD236.
P. H. Smith, J. P. D. Gow, N. J. Murray, J. H. Tutt, M. R. Soman and A. D. Holland.
Journal of Instrumentation, 9(04):P04019, 2014

[10] Quantum efficiency measurements and modeling of ion-implanted, laser-annealed charge-coupled devices: X-ray, extreme-ultraviolet, ultraviolet, and optical data
Robert A. Stern, Lawrence Shing, and Morley M. Blouke
Applied Optics Vol. 33, Issue 13, pp. 2521-2533 (1994)

[11] EUV & Soft X-ray QE Measurements of a Thinned Back-Illuminated CMOS Active Pixel Sensor
Robert A. Stern, Lawrence Shing, Nick Waltham, Andrew Harris, and Peter Pool
IEEE Electron Device Letters 32(3):354 - 356 · April 2011

[12] Electro-optic and radiation damage performance of the CIS115, an imaging sensor for the JANUS optical camera onboard JUICE
M. R. Soman ; E. A. H. Allanwood ; A. D. Holland ; K. Stefanov ; J. Pratlong ; M. Leese ; J. P. D. Gow ; D. R. Smith
Proc. SPIE 9915, High Energy, Optical, and Infrared Detectors for Astronomy VII, 991515 (August 5, 2016);
doi: 10.1117/12.2234290

[13] Found at www.cleanroom.byu.edu/OpticalCalc.phtml

[14] X-ray interactions: photoabsorption, scattering, transmission, and reflection at E=50-30000 eV, Z=1-92,
B.L. Henke, E.M. Gullikson, and J.C. Davis
Atomic Data and Nuclear Data Tables 54 no.2, 181-342 (July 1993).
Found at http://henke.lbl.gov/optical_constants/atten2.html

[15]Low-energy x-ray interaction coefficients: Photoabsorption, scattering, and reflection : E = 100-2000 eV Z = 1-94
Henke, B. L., Lee, P., Tanaka, T. J., Shimabukuro, R. L., and Fujikawa, B. K.,
Atomic Data and Nuclear Data Tables 27, 1–144 (Jan. 1982).

[16] Handbook of Optical Constants of Solids I
Palik, E. D.
Academic Press (1985).

[17] Handbook of Optical Constants of Solids II
Palik, E. D.
Academic Press (1991)

[18] Handbook of Optical Constants of Solids III
Palik, E. D.
Academic Press (1997).

[19] The X-ray energy response of silicon: Part A. Theory
G.W. Fraser, A.F. Abbey, A. Holland et al
X-ray Astronomy Group, University of Leicester
Nuclear Instruments and Methods in Physics Research A 350 (1994) 368-378

[20] Mean energy required to produce an electron-hole pair in silicon for photons of energies 50 to 1500 eV
F. Scholze,a) H. Rabus, and G. Ulm
Journal of Applied Physics Volume 84, Number 5, 1 September 1998

[21] Determination of Kilovolt Electron Energy dispersive vs Penetration Distance in Solid Materials
Everhart T.E., Hoff P. H.
J. Appl. Phys. 42, 5837 (1971)

[22] Energy Dependent Charge Spread Function In A Dedicated Synchrotron Beam pnCCD detector,
Hazem Yousef
PhD Thesis, University of Siegen, 2011

[23] Transmission, energy distribution, and SE excitation of fast electrons in thin solid films
H. J. Fitting
Phys. Stat. Sol. (a) 26, 525-535 (1974)

[24] CCD97-00 Back Illuminated 2-Phase IMO Series Electron Multiplying CCD Sensor
e2v Datasheet A1A-CCD97BI_2P_IMO Version 4, November 2011

[25] Development of an EMCCD for Lidar Applications
Bertrand de Monte, e2V
Session 28 - Detectors & Electronics
ICSO - 7th International Conference on Space Optics, 14 - 17 October 2008
Found at http://esaconferencebureau.com/icso/2008-proceedings-ppts